Thermomechanical analysis of nodule damage in HfO_2/SiO_2 multilayer coatings

Yongguang Shan (单永光)[1,2*], Hongbo He (贺洪波)[1], Chaoyang Wei (魏朝阳)[1], Ying Wang (王 营)[1,2], and Yuan'an Zhao (赵元安)[1]

[1]*Key Laboratory of High-Power Laser Materials, Shanghai Institute of Optics and Fine Mechanics, Chinese Academy of Science, Shanghai 201800, China*

[2]*Graduate University of Chinese Academy of Sciences, Beijing 100049, China*

[*]*Corresponding author: shanyg@siom.ac.cn*

Received March 14, 2011; accepted April 21, 2011; posted online July 11, 2011

Samples with nodular defects grown from gold nanoparticles are prepared, and laser-induced damage tests are conducted on them. Nodular defects, which are in critical state of damage, are cross-sectioned by focusing on the ion beam and by imaging using a field emission scanning electron microscope. The cross-sectional profile shows that cracks are generated and propagated along the nodular boundaries and the HfO_2/SiO_2 interface, or are even melted. The thermomechanical process induced by the heated seed region is analyzed based on the calculations of temperature increase and thermal stress. The numerical results give the critical temperature of the seed region and the thermal stress for crack generation, irradiated with threshold fluence. The numerical results are in good agreement with the experimental ones.

OCIS codes: 310.6870, 140.3440.
doi: 10.3788/COL201109.103101.

Nodular defect, a typical defect in multilayer coatings, largely limits the improvement of the laser-induced damage threshold (LIDT) in the nanosecond regime and thus has been widely investigated. Electric field enhancement in the nodule, induced by the microlens effect of the dome structure of nodular defects, is an important factor in reducing the LIDT[1−5]. Recently, Liu *et al.* has examined the relationship between the structure feature of the nodular defect and the resistance of laser-induced damage (LID)[6−8]. Some simple thermal stress simulations and a simple thermo-mechanical model had been developed to understand the damage mechanism of the nodular defect[9−11]. The critical condition of crack generation regarded as a damage criterion and the corresponding LIDT were given based on the average temperature of the seed zone. However, the critical temperature of crack generation, the distribution of thermal stress, and the position of crack generation remain to be elucidated.

Our previous work focused on investigating the characteristics and the electric field enhancement of nodular defects[12]. The geometric characteristics of nodular defect were determined by the seed. The height of the nodular dome and the continuity of the nodular boundary mainly determine the LIDT. The strong absorptive seed and microlens effect of the nodule play important roles in the LID of the nodule.

In this letter, samples with nodular defects grown from gold nanoparticles were prepared, LID tests were performed. The thermomechanical process induced by the heated seed zone was analyzed. The morphology of a critically damaged nodule was analyzed with a double-beam microscope (Auriga, Zeiss, Germang) which combines the functions of the focused ion beam and the field emission scanning electron microscope (FESEM).

The preparation of the samples, which are multilayer coatings with gold nanoparticles deposited on the surface of the substrate, and the details of the LID tests have been described in Ref. [12]. The total thickness of the coatings is about 4.0 μm, and the films are deposited by electron beam evaporation. The reflection coefficient of these samples is about 99% at 1 064 nm. The morphologies of nodule ejection are imaged and cross-sectioned by a double-beam microscope.

The LIDT threshold of the samples deposited with gold particles on the substrate is 7.5 J/cm^2, and that of the samples free of gold particles is 23 J/cm^2[12]. There are many unejected nodules around the nodule-ejected craters, and a typical morphology of an unejected nodule is given as shown in Fig. 1. Figure 1(a) shows an unejected nodular defect resulting from a gold particle and a crack on the surface. To examine the unejected nodule irradiated by laser, the nodule was cross-sectioned. In Fig. 1(b), the cross-sectional profile shows melting and resolidification in the seed region. Cracks have generated and propagated along the nodular boundaries and the HfO_2/SiO_2 interface. A micro-cavity has been formed above the melted region and connected with the cracks. As evidenced by the melt, the melted material can be concluded to have flown into the cracks, whereas the material has melted along the cracks.

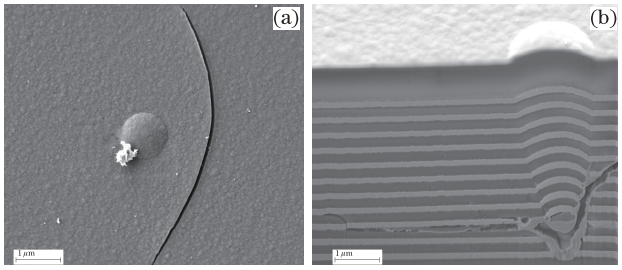

Fig. 1. FESEM image. (a) The surface morphology and (b) the profile of the same unejected nodule.

The nodule ejection is assumed to be initiated by laser energy absorption in the gold particle and spherical gold particle with a radius $a = 125$ nm embedded in an infinite homogeneous HfO_2 material. In the sphere symmetry coordinate, the temperature of the host material around the gold particle T can be calculated as[13,14]

$$\rho_{\rm h} c_{\rm h} \frac{\partial T}{\partial t} = \frac{K_{\rm h}}{r^2} \frac{\partial}{\partial r} \left(r^2 \frac{\partial T}{\partial r} \right), \tag{1}$$

where $\rho_{\rm h}$, $c_{\rm h}$, and $K_{\rm h}$ are the density, specific heat, and thermal conductivity of the host material. r is the distance from the host material to the gold particle center.

The initial and boundary conditions are $t = 0$, $T = T_0 = 300$ K, and infinity $T = T_0$. The thermal conductivity of the particle is much larger than that of the host material, so the temperature inside the particle can be assumed to be homogeneous. At the interface of the particle and the host, the power absorbed by the inclusion must be equal to the power leaving the surface by the conduction plus the rate of change in heat energy of the particle[13]

$$I_{\rm in} Q_{\rm abs} \pi a^2 = -4\pi a^2 K_{\rm h} \Big(\frac{\partial T}{\partial r} \Big)_{r=a} + \frac{4}{3} \pi a^3 \rho_{\rm p} c_{\rm p} \Big(\frac{\partial T}{\partial t} \Big)_{r=a}, \tag{2}$$

where $\rho_{\rm p}$ and $c_{\rm p}$ are the density, and specific heat of the gold particle, respectively. $I_{\rm in}$ is the laser intensity which reaches the gold particle. $Q_{\rm abs}$ is the absorption efficiency factor and is assumed to be 2 considering the microlens effect of the nodular defect and the convergent light irradiation on the gold particle. Meanwhile, localized electric field enhancement on the seed also has an important contribution to energy absorption. The laser intensity in the seed zone is expressed as

$$I_{\rm in} = m(1 - R_{\rm z}) I_0 f(t), \tag{3}$$

where I_0 is the incident light peak intensity, and $f(t)$ is the temporal distribution of the pulse. $R_{\rm z} = 99\%$ is the partial reflectivity of the mirror above the seed. $m = 4$ is the intensification factor of the laser intensity around the seed[12].

In Eq. (2), the temperature of the gold particle is assumed to be uniform throughout its volume, and the temperature of the particle equals that of the host at the surface of the particle. This assumption is justified because the particle thermal diffusion time is extremely small, which is in the order of 10^{-10} s for the gold particle with a 125-nm radius. The solution of Eq. (1) with the boundary condition Eq. (2) gives the final result for the temperature of the gold particle

$$T(a, t) = T_0 + T_\infty \left[1 - \exp(-t/\tau) \right], \tag{4}$$

and the temperature of the host material at time t and distance r from the center of the gold particle is

$$T(r, t) = T_0 + \frac{2aT_\infty}{r\sqrt{\pi}} \int_\rho^\infty \Big\{ 1 - \exp\Big[-\frac{t}{\tau} (1 - \frac{\rho^2}{x^2}) \Big] \Big\} \exp(-x^2) {\rm d}x, \tag{5}$$

where $T_\infty = I_{\rm in} Q_{\rm abs} a / 4K_{\rm h}$, $\tau = a^2 \rho_{\rm p} c_{\rm p} / 3K_{\rm h}$, and $\rho = (r - a)(4K_{\rm h} t / \rho_{\rm h} c_{\rm h})^{1/2}$.

We assume that the dynamic effects can be ignored during the heating stage, and no phase change has taken place. Therefore, the mechanical process can be analyzed by equations of the quasi-stationary thermo-elasticity theory. For a spherically symmetrical system, the thermoelasticity equation takes the following form[15]:

$$\frac{\partial}{\partial r} \left[\frac{1}{r^2} \frac{\partial}{\partial r} \left(r^2 u_{\rm r} \right) \right] = \alpha \frac{1 + \nu}{1 - \nu} \frac{\partial T(r, t)}{\partial r}, \tag{6}$$

where $u_{\rm r}$ is the radial component of the displacement vector, ν is the Poisson ratio, and α is the thermal expansion coefficient. The relations between strains and stress have the following forms in a spherical symmetry system:

$$\begin{cases} \varepsilon_{\rm r} = \dfrac{\partial u_{\rm r}}{\partial r} = \dfrac{1}{E} \left[\sigma_{\rm r} - 2\nu \sigma_\theta \right] + \alpha T(r, t) \\ \varepsilon_\theta = \dfrac{u_{\rm r}}{r} = \dfrac{1}{E} \left[\sigma_\theta - \nu (\sigma_\theta + \sigma_{\rm r}) \right] + \alpha T(r, t) \end{cases}, \tag{7}$$

where E is Young's modulus, ε is the strain, and σ is the stress. The subscripts r and θ denote the radial and tangential directions. After two integrals were carried out on Eq. (5), the following can be obtained by

$$u_{\rm r}(r, t) = \alpha \frac{1 + \nu}{1 - \nu} \frac{1}{r^2} \int_0^r T(r, t) r^2 {\rm d}r + C_1 r + \frac{C_2}{r^2}, \tag{8}$$

where C_1 and C_2 are the integral constants and are determined by boundary conditions. $u_{\rm r}(0, t) = 0$, so $C_2 = 0$. $\sigma_{\rm r}(\infty, t) = 0$ and $u_{\rm r}(\infty, t) = 0$, so $C_1 = 0$. From Eqs. (6) and (7), the tangential stress can be obtained by

$$\sigma_\theta(r, t) = \frac{\alpha E}{1 - \nu} \frac{1}{r^3} \int_0^r T(x, t) x^2 {\rm d}x - \frac{\alpha E T(r, t)}{1 - \nu}. \tag{9}$$

According to the Griffith criterion, the linear elastic theory of crack propagation, the critical stress level takes the following form[16]:

$$\sigma_{\rm c} = \sqrt{EG / \pi r_0}, \tag{10}$$

where $\sigma_{\rm c}$ is the critical stress for a body containing an internal crack of length $2r_0$, E is the Young's modulus of the host material, and G is the energy release rate. Equation (10) indicates that the critical stress level decreases with the crack length.

In this letter, the length of crack $2r_0$ is taken to be $2a$, the diameter of the gold seed, and the stress is the tangential tensile stress σ_θ. When the condition $\sigma_\theta \geqslant \sigma_{\rm c}$ is satisfied, crack growth would occur around the seed.

From Eq. (5), the physical parameters used in the calculation are listed in Table 1[20]. Obtaining the numerical results is easy. The temperature distribution in the radial direction, irradiated with threshold fluence 7.5 J/cm^2, is shown in Fig. 2. The maximal temperature of the seed zone is 3 280 K at the end of 12-ns pulse. The maximal temperature, corresponding to the LIDT, is the critical temperature of the seed zone for nodule damage. From the temperature distribution in the radial direction, if the critical temperature of the inelastic deformation of the HfO_2 material is assumed to be 1 924 K, the corresponding radial position is 0.25 μm. Therefore, the thermoelasticity of solids can be applied to the range where the temperature is below 1 924 K.

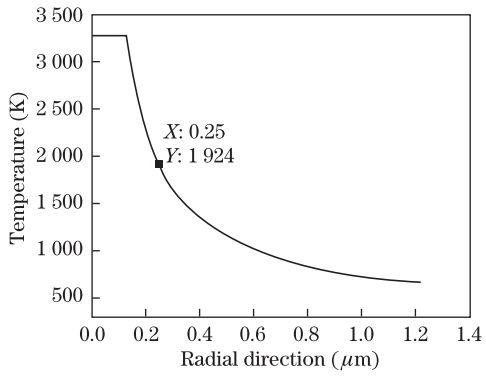

Fig. 2. Temperature distribution in the radial direction under the irradiation of threshold fluence.

Table 1. Main Parameters Used in the Numerical Calculations[20]

Parameter	HfO_2	Gold
Thermal Expansion Coefficient (K)	3.8×10^{-6}	14.2×10^{-6}
Thermal Conductivity (W/m· K)	4.3	311
Specific Heat (J/(kg·K))	340	131
Melting Point (K)	3 031	1 336
Boiling Point (K)	5 673	3 090
Density (kg/m^3)	9 680	19 300
Young Modulus (GPa)	76	79
Poisson's Ratio	0.27(ZrO_2)	0.44
Energy Release Rate (J/m^2)	1	

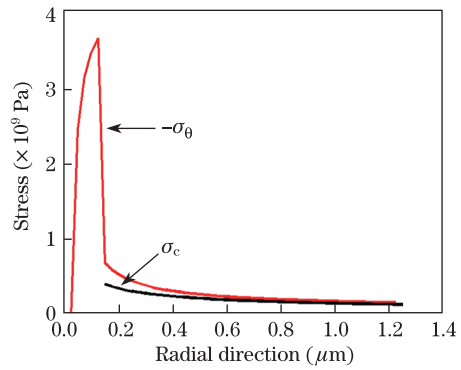

Fig. 3. Distribution of tangential stress in the radial direction at the end of 12-ns pulse.

The tangential stress and the critical tensile stress in the radial direction can be calculated from Eqs. (9) and (10). At the end of the 12-ns pulse of threshold fluence, the tangential stress distribution is shown in Fig. 3. The tangential stress is larger than the critical value of the host material from 0.25 to 1.200 μm. This indicates that crack generation occurs in this range. This result is in good agreement with the cracks shown in Fig. 2.

According to the numerical results, the cracks should have propagated in all directions for the spherical symmetrical system. However, the cracks just propagate along the nodular boundaries and the HfO_2/SiO_2 interface as shown in Fig. 1(b). This phenomenon is related to the structure feature of the nodule and interface[17]. Recently, Liu *et al.* has observed that the boundary region between the nodular defect and the surrounding layers changes as the deposition progresses. Close to the seed, the boundary region is completely discontinuous. However, as more materials are deposited, the boundaries heal and tend to be continuous[6]. The mechanical properties of the nodular boundaries have undesirable effects, and cracks are initiated at the nodules when the coatings are stressed by mechanical forces[16,18]. This is why crack generation and propagation have the tendency to take place along the nodular boundaries when the thermal stress is loaded by the heated seed.

Once crack growth takes place, on one hand, the internal elastic potential energy is partly released, and the tangential stress is decreased; on the other hand, the critical tensile stress σ_c also decreases due to the length of crack increase. If the condition $\sigma_\theta \geqslant \sigma_c$ is still satisfied at the crack tip, the crack will continue to extend until the condition is broken.

From the above, the thermomechanical analysis of the critical conditions of nodule damage agree with our experimental findings. However, theoretical analysis is just qualitative analysis, and the assumption on the absorption efficiency factor Q_{abs} needs to be proven.

The whole process of defect-initiated damage is complex and involves the electrodynamics, thermodynamics, and mechanics of continuous materials. Bonneau *et al.* have performed numerical simulations on the damage process of ultraviolet (UV), laser interaction with gold nanoparticles, including energy absorption, crack formation, and propagation leading to craters[19]. Their numerical and experimental results agree well, but the numerical analysis is complicated. From the critical conditions of nodule damage, we can conclude with our model that cracks start generating irradiated with threshold fluence based on the analysis of temperature rise and stress distribution. This model gives a concise and effective way to analyze qualitatively the critical conditions of nodule-initiated damage.

In conclusion, based on the calculation of temperature rise and the corresponding thermal stress, the thermomechanical process of nodule damage is analyzed. The numerical temperature of nodule damage is about 3 300 K in the seed region, and the tangential stress loaded by the heated seed region can induce crack generation, irradiated with threshold fluence. The numerical results can explain well the experimental phenomena.

References

1. C. J. Stolz, M. D. Feit, and T. V. Pistor, Appl. Opt. **45,** 1594 (2006).
2. Y. Wang, Y. Zhang, X. Liu, W. Chen, and P. Gu, Opt. Commun. **278,** 317 (2007).
3. C. J. Stolz, S. Hafeman, and T. V. Pistor, Appl. Opt. **47,** C162 (2008).
4. J. R. Milward, K. L. Lewis, K. Sheach, and R. A. Heinecke, Proc. SPIE **2114,** 309 (1993).
5. J. F. DeFord and M. R. Kozlowski, Proc. SPIE **1848,** 455 (1992).
6. X. Liu, D. Li, Y. Zhao, and X. Li, Appl. Opt. **49,** 1774 (2010).
7. X. Liu, D. Li, Y. Zhao, X. Li, and J. Shao, Appl. Surf. Sci. **256,** 3783 (2010).

8. X. Liu, D. Li, Y. Zhao, X. Li, X. Ling, and J. Shao, Chin. Opt. Lett. **8,** 41 (2010).
9. X. Ling, J. Shao, and Z. Fan, J. Vac. Sci. Technol. A **27,** 183 (2009).
10. J. Dijon, M. Poulingue, and J. Hue, Proc. SPIE **3578,** 387 (1999).
11. R. Sawicki, C. Shang, and T. Swatloski, Proc. SPIE **2428,** 333 (1994).
12. Y. Shan, H. He, C. Wei, S. Li, M. Zhou, D. Li, and Y. Zhao, Appl. Opt. **49,** 4290 (2010).
13. C. H. Chan, Appl. Phys. Lett. **26,** 628 (1975).
14. C. Wei, J. Shao, H. He, K. Yi, and Z. Fan, Opt. Express **16,** 3376 (2008).
15. Y. Takeuti, *Thermal Stress* (in Chinese) (Science, Beijing, 1977).
16. M. Poulingue, J. Dijon, M. Ignat, H. Leplan, and B. Pinot, Proc. SPIE **3578,** 370 (1999).
17. J. Dijon, G. Ravel, and B. Andre, Proc. SPIE **3578,** 398 (1999).
18. T. Spalvins and W. A. Brainard, J. Vac. Sci. Technol. **11,** 1186 (1974).
19. F. Bonneau, P. Combis, J. L. Rullier, J. Vierne, B. Bertussi, M. Commandre, L. Gallais, J. Y. Ntoli, I. Bertron, F. Malaise, and J. T. Donohue, Appl. Phys. B **78,** 447 (2004).
20. C. Stolz, F. Genin, T. Reitter, N. Molau, R. Bevis, M. Gunten, D. Smith, and J. Anzellotti, Proc. SPIE **2966,** 265 (1997).